Spin Electronics

Effects of Growth Order on Perpendicular Magnetic Anisotropy of Heavy-Metal/Ferromagnet/MgO Trilayered Structures

Yuejie Zhang[1,2], Xiaofei Yang[1], Peng Li[2], Jun Ouyang[1], and Mingzhong Wu[2*]

[1] School of Optical and Electronic Information, Huazhong University of Science and Technology, Wuhan 430074, China
[2] Department of Physics, Colorado State University, Fort Collins, CO 80523, USA
* Senior Member, IEEE

Received 20 Feb 2019, accepted 15 Mar 2019, published 29 Apr 2019, current version 28 May 2019.

Abstract—Previous experiments have shown that perpendicular magnetic anisotropy (PMA) in trilayers consisting of a CoFeB layer, an MgO layer, and a nonmagnetic metal (NM) layer depends strongly on whether the CoFeB layer was grown on the top of an NM layer or was capped by an NM layer. In this letter, we study the physical origin of this phenomenon through first-principles calculations. We took MgO/CoFe/Ta and Ta/CoFe/MgO as model structures and analyzed the magnetic anisotropy energy (MAE) therein. The "substrate/Ta/CoFe/MgO" structure had a notably higher MAE than the "substrate/MgO/CoFe/Ta" structure. This difference results mainly from different stresses in the Ta layers, and the latter gives rise to a difference in the hybridization strength of in-plane orbits (d_{xy}, $d_{x^2-y^2}$, p_x, and p_y). The p-orbital hybridization in the Ta layers contributes significantly to the PMA in both structures.

Index Terms—Spin electronics, nanomagnetics, information storage, coupled phenomena.

I. INTRODUCTION

Magnetic tunnel junctions (**MTJ**s) with ferromagnetic layers possessing perpendicular magnetic anisotropy (**PMA**) have attracted considerable attention in recent years [Metaxas 2007, Ikeda 2010, Gmitra 2013, Hotta 2013, Baek 2018]. Strong magnetic anisotropy energy (**MAE**) is highly desirable in order to obtain nonvolatile memory with high density and high stability [Gambardella 2003, Khajetoorians 2014, Rau 2014, Yu 2014, Ou 2015]. Over the past few years [Cheng 2011, Wang 2011, Peng 2015, 2017], one of the main efforts has been on the study of the impact of different 5d and 4d nonmagnetic metals (**NM**s) on the PMA strength in MgO/ferromagnetic metal (**FM**)/NM layered heterostructures. MgO/FM/NM and NM/FM/MgO are assumed to be identical in previous studies using first-principles calculations [Peng 2015, 2017], but experiments have shown that there are notable differences between the properties of MgO/CoFe/NM and NM/CoFe/MgO structures. For example, PMA in MgO/CoFe/NM structures can be more sensitive to temperature than NM/CoFe/MgO counterparts [Cheng 2011, Wang 2011]. In Cheng [2011], it was reported that in a MgO/CoFeB/Ta structure, Ta may diffuse into the CoFeB layer and replace boron therein, causing a deterioration of the CoFeB layer at the Ta/CoFeB interface. This may result in a difference in the PMA field of the MgO/CoFeB/Ta structure and its inverted structure. The physical reasons for such PMA differences are still unknown.

The use of the Ta/CoFe/MgO structure to calculate the MAE was considered in Ong [2015a, 2015b], which concluded that an expansive strain on the FM layer leads to a weaker MAE. Thus, the analysis presented here is consistent with the previous findings. In general, strong PMA can result from high spin–orbit coupling (**SOC**) energy, a special ligand field, and a large orbital moment [Khajetoorians 2014, Ou 2015, Rau 2014]. In this letter, using MgO/CoFe/Ta and Ta/CoFe/MgO as model structures, we study the origins of different types of PMA via first-principles calculations. Our calculations showed that the MAE in a "substrate/Ta/CoFe/MgO" structure (Ta/CoFe) is higher than in a "substrate/MgO/CoFe/Ta" structure (CoFe/Ta). We found that this difference results mainly from the different stresses in the Ta layers. We also confirmed that p-orbital hybridization in Ta contributes significantly to PMA in both the structures. Our results point a path to optimize PMA devices through interface engineering.

Corresponding authors: Peng Li and Jun Ouyang (e-mail: lipengest@hotmail.com; oyj@hust.edu.cn).
Digital Object Identifier 10.1109/LMAG.2019.2914007

II. CALCULATION METHOD

Our first-principles calculations were performed by using the Vienna *ab initio* simulation package (**VASP**) [Kresse 1993, Dong 1996], with a generalized gradient approximation and the projector augmented wave (**PAW**) potentials [Blöchl 1994]. The structures were fully relaxed until the residual forces were less than 0.01 eV/Å. We used a cutoff energy of 540 eV and a K-point mesh of $20 \times 20 \times 1$, which are sufficient to ensure a good convergence of the MAE. Different thin-film growth orders were considered. If Ta is grown first, the properties of the CoFe layer depend heavily on the top surface of the Ta layer, whereas in the reversed order, when the MgO layer is grown first, the interfacial structure of the CoFe layer depends on the top surface of the MgO layer. Considering this fact, in our calculations, the in-plane lattice constants of the CoFe/Ta layers were calculated based on the bulk MgO, whereas those of the Ta/CoFe layers were based on the bulk Ta. A 15 Å thick vacuum layer is included on the top of the two structures. The layered structures of MgO/CoFe/Ta and Ta/CoFe/MgO are shown schematically in Fig. 1(a) and (b), respectively.

Compared to the CoFe/MgO interface that contributes to an MAE with an average of 0.16 erg/cm^2 [Peng 2015, 2017], the CoFe/Ta interface contributes to a significant amount of MAE (1.54 erg/cm^2)

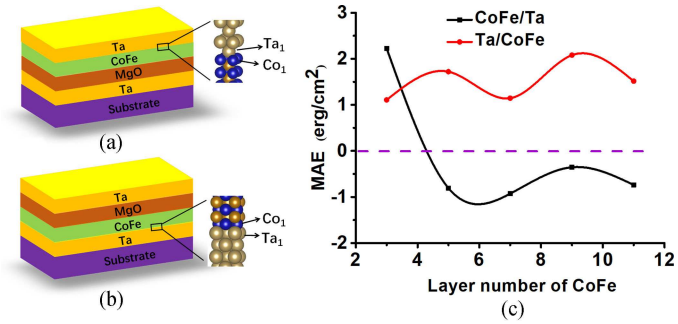

Fig. 1. (a) and (b) Schematics of crystalline structures for MgO/CoFe/Ta and Ta/CoFe/MgO, respectively. The a-series is the MgO/CoFe(t)/Ta structure, and the b-series is the Ta/CoFe(t)/MgO structure. (c) MAE as a function of the atomic layer number of CoFe. The x-axis is the number of the CoFe layers in CoFe(t)/Ta or Ta/CoFe(t) structure. The y-axis is the total MAE per unit area. PMA is positive, and in-plane MAE is negative.

[Peng 2015, 2017]. Thus, in this letter, we assume that the MgO/CoFe structure and the CoFe/MgO structure are the same by default. We focus on the difference between the Ta/CoFe and CoFe/Ta structures in the following.

III. RESULTS AND DISCUSSION

Previous calculations [Ong 2015a, 2015b, Peng 2015, 2017, Odkhuu 2016] have confirmed that three to five layers of Ta monolayers are sufficient for PMA. Here, we use four layers of Ta in all structures. The thickness of CoFe varies from three monolayers to 11 monolayers. The MAE is determined as the difference of the total energies when the magnetization orients along the in-plane ([100]) and perpendicular ([001]) directions, taking the SOC into account as [Ong 2015b, Peng 2015, 2017, Odkhuu 2016]

$$\mathrm{MAE} = \xi^2 \sum_{o,u} \left[\frac{|\langle \psi_o | L_z | \psi_u \rangle|^2}{E_u - E_o} - \frac{|\langle \psi_o | L_x | \psi_u \rangle|^2}{E_u - E_o} \right] \quad (1)$$

where $\psi_o(\psi_u)$ and $E_o(E_u)$ represent eigenstates and eigenvalues, respectively, and ξ is the SOC constant. We calculated the MAE of the CoFe/Ta and Ta/CoFe structures, and the results are shown in Fig. 1(c).

In Fig. 1(c), the easy axis of the CoFe(3)/Ta(4) structure is out-of-plane, but with an increase in the CoFe thickness, the easy axis of CoFe (5)/Ta(4) has changed to in-plane. The Ta/CoFe(t) structure has its easy axis out-of-plane for all the thicknesses considered here. Both structures show an oscillation of MAE regarding the CoFe thickness [Yin 2017]. The spin–orbit term is evaluated using the second-order approximation [Kim 2009, Collet 2017] implemented in VASP

$$H_{\mathrm{SOC}} = \frac{\hbar^2}{4m^2c^2} \frac{1}{r} \frac{\partial V}{\partial r} \vec{L} \cdot \vec{s} \quad (2)$$

where $\vec{L}$ is the angular-momentum operator, $\vec{s}$ are the Pauli spin matrices, and V is the spherical part of the all-electron Kohn–Sham potential inside the PAW spheres. According to (2), the SOC energies of a-series and b-series of different CoFe thickness are calculated, which are shown in Fig. 2(a). The SOC energies from the Co_6 layer to Co_1 layer are consistent in CoFe/Ta and Ta/CoFe structures. Interestingly, the Ta layers from the Ta_1 layer to Ta_4 are completely different. In other words, the b-series of the Ta layers has a stronger SOC energy

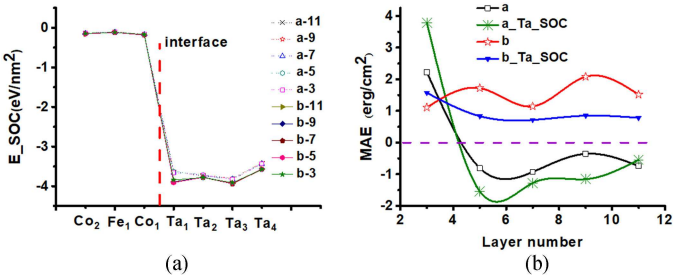

Fig. 2. (a) SOC energy difference of a-series and b-series mainly comes from heavy metal Ta. The SOC energies of FM layers are consistent in CoFe/Ta and Ta/CoFe structures. Data from Co_2 layer to Co_1 layer are shown. Ta_x ($x = 1, 3, \ldots$) represents the first and third layers at the CoFe/Ta interface or Ta/CoFe interface. Similarly, Fe_x ($x = 1, 2, \ldots$) and Co_x ($x = 1, 2, \ldots$). (b) Heavy metal MAE versus total structure MAE. The MAE difference between a-series and b-series is mainly due to the huge MAE difference in heavy metal Ta.

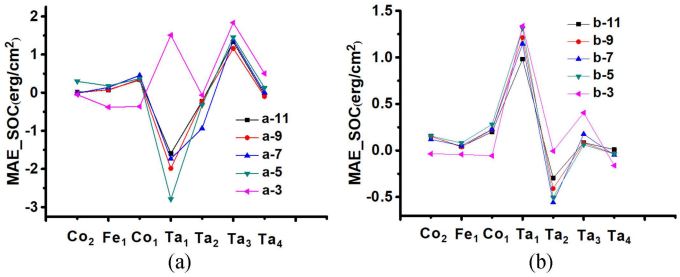

Fig. 3. The MAE is mainly provided by the Ta_1 layer in a-series and b-series. The MAE of FM layers are consistent in CoFe/Ta and Ta/CoFe structures. Data from the Co_2 layer to Co_1 layer are shown. Positive is PMA, negative is in-plane MAE.

than the a-series, which may be the main reason for the different MAE between a-series and b-series.

The magnetic anisotropy difference between the a-series and the b-series for Ta is as high as 2 erg/cm^2, as shown in Fig. 2(b). The MAEs of SOC energy from Ta is as high as -1.5 erg/cm^2 in CoFe(t)/Ta. Except for the CoFe(3)/Ta, the MAEs of CoFe(t)/Ta ($t = 5, 7, 9, 11$) is about -0.9 erg/cm^2. However, for Ta/CoFe(t) structures, the MAEs of SOC energy of Ta is as high as 1.1 erg/cm^2, which are consistent with previous calculations [Peng 2015, 2017]. These results show that the MAEs of CoFe(t)/Ta and Ta/CoFe(t) structures is dominated by Ta.

In order to further study the difference in Ta for CoFe(t)/Ta and Ta/CoFe(t), in the following, we calculated monolayer MAE. In Fig. 3(a), the MAE of each layer Ta is larger than the MAE of each layer CoFe in the five CoFe(t)/Ta structures, but the largest MAE is from the Ta_1 layer, and the MAEs of the CoFe(t)/Ta structures mainly come from Ta_1. In Fig. 3(b), the MAEs of the Ta/CoFe(t) structures mainly come from Ta_1, and the conclusion in Fig. 3(b) is similar to that in Fig. 3(a). The SOC energy of the Ta_1 layer mainly contributes to the PMA in the CoFe(3)/Ta structure, and the Ta_1 layer of the other structures ($t > 3$) is in-plane MAEs. However, the Ta_1 layers of Ta/CoFe($t = 3, 5, 7, 9, 11$) structures are the PMA.

In order to understand the Ta_1 layers further, a detailed orbital-resolved analysis is performed for the Ta_1 layer as MAEs at CoFe(t)/Ta and Ta/CoFe(t) structures. The MAEs of CoFe(t)/Ta ($t = 5, 7, 9, 11$ except for $t = 3$) prefer in-plane magnetization, but MAEs of Ta/CoFe(t) ($t = 3, 5, 7, 9, 11$) prefer PMA. According to the particularities of

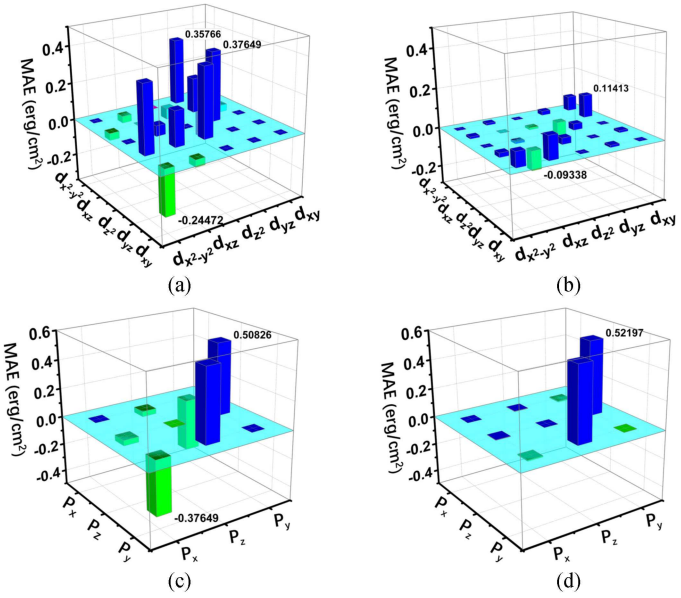

Fig. 4. Orbital-resolved MAE of the Ta_1 layer in CoFe(3)/Ta and Ta/CoFe(3) structures. Blue columns represent positive contributions to PMA, and green columns represent negative contributions to PMA. (a) and (c) CoFe(3)/Ta structure. (b) and (d) Ta/CoFe(3) structure.

MAE in CoFe(t)/Ta and Ta/CoFe(t) structures, we choose CoFe(3)/Ta and Ta/CoFe(3) for more detailed study.

In Fig. 4, we show the orbital-resolved MAEs of the Ta_1 in CoFe(3)/Ta and Ta/CoFe(3) structures, where matrix elements, for example (d_{xy}, d_{yz}), denote the hybridization between two orbitals via SOC. According to (1), the matrix element of $L_z(L_x)$ provides a positive (negative) contribution to PMA. As a result, positive contributions from $\langle L_z\rangle$ exceed negative ones from $\langle L_x\rangle$, leading to MAE with positive K_i. One can see clearly that the largest positive contribution to PMA for the Ta_1 in CoFe(3)/Ta [see Fig. 4(a)] comes from the matrix elements (d_{z^2},d_{yz}) and ($d_{x^2-y^2}$,d_{yz}), which means that $\langle d_{z^2}|L_z|d_{yz}\rangle$ ($\langle d_{x^2-y^2}|L_z|d_{yz}\rangle$) is much bigger than $\langle d_{z^2}|L_x|d_{yz}\rangle$($\langle d_{x^2-y^2}|L_x|d_{yz}\rangle$), of which the matrix element ($d_{x^2-y^2}$,d_{xy}) provides negative contribution to PMA. In the Ta/CoFe(3) structure [see Fig. 4(b)], the matrix element ($d_{x^2-y^2}$,d_{xy}) provides positive contribution to PMA, and (d_{xz},d_{yz}) provides negative contribution. Previous studies have found that the contribution of p-orbital hybridization to PMA in Ta is larger than that of d-orbital hybridization to PMA [Peng 2015, 2017]. We calculated the contribution of p-orbital hybridization to PMA in two structural systems, as shown in Fig.4 (c) and (d). The matrix element (p_y,p_z) provides an extremely large positive contribution to PMA in both the CoFe(3)/Ta and Ta/CoFe(3) structures. The contribution of matrix element (p_x,p_y) to MAE is almost zero in Ta/CoFe(3), whereas in CoFe(3)/Ta, it is -0.376 erg/cm^2. Thus, it can be concluded that the PMA of Ta/CoFe(3) mainly comes from the p-orbital hybridization, but for the CoFe (3)/Ta structure, the PMA mainly comes from p- and d-orbitals, which is different from previous related reports.

In the CoFe(t)/Ta structure, the CoFe film is grown on MgO with a lattice constant up to 4.2112 Å [Karki 1997], Ta is 3.3026 Å [Mueller 1977] and CoFe is the smaller lattice constant than that of MgO and Ta. When the CoFe film is thin, the interatomic spacings between the CoFe atoms are large, so Ta atoms are grown in deep interatomic

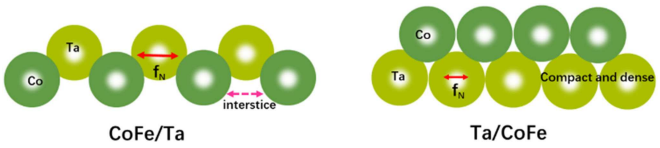

Fig. 5. CoFe/Ta and Ta/CoFe interfacial structures.

spacings between CoFe atoms, as shown in Fig. 5, The pressure on the in-plane orbits (d_{xy},$d_{x^2-y^2}$, and p_x,p_y) is relatively high. In Fig. 4(a) and (b), the hybrid strength of in-plane orbits matrix elements (p_x,p_y) and (d_{xy},$d_{x^2-y^2}$) is significantly greater in the CoFe(3)/Ta structure than that in Ta/CoFe(3) structure. With the CoFe thickness increasing, the lattice constant of ultrathin CoFe begins to shrink and gradually approaches the lattice constants of block CoFe. The stress at the CoFe interface also begins to increase and extends to the Ta interface. The in-plane orbital pressure of Ta_1 layer is increasing with the thickness of CoFe increasing. Therefore, the PMA of CoFe/Ta structure is very sensitive to the CoFe thickness, which is completely consistent with the conclusion of the experiment [Cheng 2011, Wang 2011].

If Ta is grown first, the CoFe layer depends on the top surface of Ta. When the CoFe film is very thin, Ta keeps its original structure; CoFe atoms are grown on the surface of Ta, which is dense and has relatively small atomic interatomic spacings, as shown in Fig. 5. Therefore, Ta hybrid orbits are mostly vertical in Ta/CoFe(t) structures, such as d_{xz},d_{yz},d_{z^2}, and p_z, which can be explained by Fig. 4. The matrix elements (p_x,p_y) and (d_{xy},$d_{x^2-y^2}$) provide MAE energies of -0.376 and -0.24 erg/cm^2 for PMA in CoFe(3)/Ta structure, whereas they are -0.01 and 0.45 erg/cm^2 in Ta/CoFe(3). Therefore, the CoFe thickness in the appropriate range will not have a significant impact on the PMA in Ta/CoFe(t) structure, which is completely consistent with the conclusion of the experiment [Cheng 2011, Wang 2011].

IV. CONCLUSION

In this letter, we investigated SOC-associated MAE in CoFe/Ta and Ta/CoFe structures. We found that the different MAEs between the CoFe/Ta and Ta/CoFe structures are mainly due to the regulation of CoFe interface stress for Ta. In CoFe/Ta, with an increase in the CoFe thickness, the in-plane compressive stress also increases. This is because the Ta layer is grown on the CoFe layer, in-plane compressive stress is easily passed to the first Ta layer, and the in-plane orbital coupling enhancement of Ta is realized. In Ta/CoFe structure, however, the situation is completely different. Since Ta is grown first, the surface stress of the CoFe film increases with an increase in the CoFe thickness. However, the surface of the Ta film is compact and dense, and the CoFe surface stress is difficult to change the surface structure of the Ta film. Therefore, the CoFe thickness in the appropriate range will not have a significant impact on PMA in the Ta/CoFe structure.

ACKNOWLEDGMENT

This work was supported in part by the National Natural Science Foundation of China under Grant 11574096, in part by the Graduates' Innovation Fund, Huazhong University of Science and Technology under Grant 5003182006, in part by the U.S. National Science Foundation under Grant EFMA-1641989, and in part by the U.S. Department of Energy, Office of Science, Basic Energy Sciences under Grant DE-SC0018994. The authors thank Prof. L. Miao at the Huazhong University of Science and Technology for discussions on the calculations.

REFERENCES

Baek S-H C, Amin V P, Oh Y-W, Go G, Lee S-J, Lee G-H, Kim K-J, Stiles M D, Park B-G, Lee K-J (2018), "Spin currents and spin–orbit torques in ferromagnetic trilayers," *Nature Mater.*, vol. 17, pp. 509–513, doi: 10.1038/s41563-018-0041-5.

Blöchl P E (1994), "Projector augmented-wave method," *Phys. Rev. B*, vol. 50, pp. 17953–17979, doi: 10.1103/PhysRevB.50.17953.

Cheng C-W, Feng W, Chern G, Lee C M, Wu T-H (2011), "Effect of cap layer thickness on the perpendicular magnetic anisotropy in top MgO/CoFeB/Ta structures," *J. Appl. Phys.*, vol. 110, 033916, doi: 10.1063/1.3621353.

Collet M, Mattana R, Moussy J-B, Ollefs K, Collin S, Deranlot C, Anane A, Cros V, Petroff F, Wilhelm F, Rogalev A (2017), "Investigating magnetic proximity effects at ferrite/Pt interfaces," *Appl. Phys. Lett.*, vol. 111, pp. 202401-1–202401-4, doi: 10.1063/1.4987145.

Dong W, Kresse G, Furthmüller J, Hafner J (1996), "Chemisorption of H on Pd(111): An *ab initio* approach with ultrasoft pseudopotentials," *Phys. Rev. B*, vol. 54, pp. 2157–2166, doi: 10.1103/PhysRevB.54.2157.

Gambardella P, Rusponi S, Veronese M, Dhesi S S, Grazioli C, Dallmeyer A, Cabria I, Zeller R, Dederichs P H, Kern K, Carbone C, Brune H (2003), "Giant magnetic anisotropy of single cobalt atoms and nanoparticles," *Science*, vol. 300, pp. 1130–1133, doi: 10.1126/science.1082857.

Gmitra M, Matos-Abiague A, Draxl C, Fabian J (2013), "Magnetic control of spin-orbit fields: A first-principles study of Fe/GaAs junctions," *Phys. Rev. Lett.*, vol. 111, 036603, doi: 10.1103/PhysRevLett.111.036603.

Hotta K, Nakamura K, Akiyama T, Ito T, Oguchi T, Freeman A J (2013), "Atomic-layer alignment tuning for giant perpendicular magnetocrystalline anisotropy of 3d transition-metal thin films," *Phys. Rev. Lett.*, vol. 110, 267206, doi: 10.1103/PhysRevLett.110.267206.

Ikeda S, Miura K, Yamamoto H, Mizunuma K, Gan H D, Endo M, Kanai S, Hayakawa J, Matsukura F, Ohno H (2010), "A perpendicular-anisotropy CoFeB–MgO magnetic tunnel junction," *Nature Mater.*, vol. 9, pp. 721–724, doi: 10.1038/NMAT2804.

Karki B B, Stixrude L, Clark S J, Warren M C, Ackland G J, Crain J (1997), "Structure and elasticity of MgO at high pressure," *Amer. Mineral.*, vol. 82, pp. 51–60, doi: 10.2138/am-1997-1-207.

Khajetoorians A A, Wiebe J (2014), "Hitting the limit of magnetic anisotropy," *Science*, vol. 344, pp. 976–977, doi: 10.1126/science.1254402.

Kim Y-S, Hummer K, Kresse G (2009), "Accurate band structures and effective masses for InP, InAs, and InSb using hybrid functionals," *Phys. Rev. B*, vol. 80, pp. 035203-1–035203-9, doi: 10.1103/PhysRevB.80.035203.

Kresse G, Hafner J (1993), "*Ab initio* molecular dynamics for open-shell transition metals," *Phys. Rev. B*, vol. 48, pp. 13115–13118, doi: 10.1103/PhysRevB.48.13115.

Kresse G, Hafner J (1993), "*Ab initio* molecular dynamics for liquid metals," *Phys. Rev. B*, vol. 47, pp. 559–561, doi: 10.1103/PhysRevB.47.558.

Metaxas P J, Jamet J P, Mougin A, Cormier M, Ferré J, Baltz V, Rodmacq B, Dieny B, Stamps R L (2007), "Creep and flow regimes of magnetic domain wall motion in ultrathin Pt/Co/Pt films with perpendicular anisotropy," *Phys. Rev. Lett.*, vol. 99, 217208, doi: 10.1103/PhysRevLett.99.217208.

Mueller M H (1977), "Lattice parameter of tantalum," *Scripta Metallurgica*, vol. 11, doi: 10.1016/0036-9748(77)90141-7.

Odkhuu D (2016), "Giant strain control of magnetoelectric effect in Ta/Fe/MgO," *Sci. Rep.*, vol. 6, 32742, doi: 10.1038/srep32742.

Ong P V, Kioussis N, Amiri P K, Wang K L, Carman G P (2015a), "Strain control magnetocrystalline anisotropy of Ta/FeCo/MgO heterostructures," *J. Appl. Phys.*, vol. 117, 17B518-1, doi: 10.1063/1.4916115.

Ong P V, Kioussis N, Odkhuu D, Amiri P K, Wang K L, Carman G P (2015b), "Giant voltage modulation of magnetic anisotropy in strained heavy metal/magnet/insulator heterostructures," *Phys. Rev. B*, vol. 92, 020407, doi: 10.1103/PhysRevB.92.020407.

Ou X, Wang H, Fan F, Li Z, Wu H (2015), "Giant magnetic anisotropy of Co, Ru, and Os adatoms on MgO (001) surface," *Phys. Rev. Lett.*, vol. 115, 257201, doi: 10.1103/PhysRevLett.115.257201.

Peng S, Wang M, Yang H, Zeng L, Nan J, Zhou J, Zhang Y, Hallal A, Chshiev M, Wang K L, Zhang Q, Zhao W (2015), "Origin of interfacial perpendicular magnetic anisotropy in MgO/CoFe/metallic capping layer structures," *Sci. Rep.*, vol. 5, 18173, doi: 10.1038/srep18173.

Peng S, Zhao W, Qiao J, Su L, Zhou J, Yang H, Zhang Q, Zhang Y, Grezes C, Amiri P K, Wang K L (2017), "Giant interfacial perpendicular magnetic anisotropy in MgO/CoFe/capping layer structures," *Appl. Phys. Lett.*, vol. 110, 072403, doi: 10.1063/1.4976517.

Qviller A J, Magnus F, Kirby B J, Hjörvarsson B, Frommen C, Hauback B C (2018), "Direct observation of the magnetic proximity effect in amorphous exchange-spring magnets by neutron reflectometry," unpublished paper. [Online]. Available: https://arxiv.org/abs/1804.01479

Rau I G, Baumann S, Rusponi S, Donati F, Stepanow S, Gragnaniello L, Dreiser J, Piamonteze C, Nolting F, Gangopadhyay S, Albertini O R, Macfarlane R M, Lutz C P, Jones B A, Gambardella P, Heinrich A J, Brune H (2014), "Reaching the magnetic anisotropy limit of a 3d metal atom," *Science*, vol. 344, pp. 988–992, doi: 10.1126/science.1252841.

Wang W X, Yang Y, Naganuma H, Ando Y, Yu R C, Han X F (2011), "The perpendicular anisotropy of $Co_{40}Fe_{40}B_{20}$ sandwiched between Ta and MgO layers and its application in CoFeB/MgO/CoFeB tunnel junction," *Appl. Phys. Lett.*, vol. 99, 012502, doi: 10.1063/1.3605564.

Yin L, Wang X, Mi W (2017), "Electric-field tunable perpendicular magnetic anisotropy in tetragonal $Fe_4N/BiFeO_3$ heterostructures," *Appl. Phys. Lett.*, vol. 111, 032404, doi: 10.1063/1.4993907.

Yu G, Upadhyaya P, Fan Y, Alzate J G, Jiang W, Wong K L, Takei S, Bender S A, Chang L-T, Jiang Y, Lang M, Tang J, Wang Y, Tserkovnyak Y, Amiri P K, Wang K L (2014), "Switching of perpendicular magnetization by spin–orbit torques in the absence of external magnetic fields," *Nature Nanotechnol.*, vol. 9, pp. 548–554, doi: 10.1038/NNANO.2014.94.

Zhou X, Ma L, Shi Z, Fan W J, Zheng J-G, Evans R F L, Zhou S M (2015), "Magnetotransport in metal/insulating-ferromagnet heterostructures: Spin Hall magnetoresistance or magnetic proximity effect," *Phys. Rev. B*, vol. 92, 060402, doi: 10.1103/PhysRevB.92.060402.